JOURNAL OF PROPULSION AND POWER
Vol. 16, No. 3, May–June 2000

Effects of Radial Location on the Migration of Hot Streaks in a Turbine

Karen L. Gundy-Burlet*
NASA Ames Research Center, Moffett Field, California 94035-1000
and
Daniel J. Dorney†
Virginia Commonwealth University, Richmond, Virginia 23284-3105

Experimental data have shown that combustor temperature nonuniformities can lead to the excessive heating of first-stage rotor blades in turbines. This heating of the rotor blades can lead to thermal fatigue and degrade turbine performance. The results of recent studies have shown that variations in the circumferential location, or clocking, of the first-stage stator airfoils can be used to control the adverse effects of the hot streaks by mixing hot streak fluid with the cooler fluid contained in the first-stage stator wake. Less emphasis has been placed on determining the optimal radial location of the hot streaks at the inlet to the first-stage stator blade row. In the present investigation, three-dimensional unsteady Navier–Stokes simulations have been performed for a $1\frac{1}{2}$-stage high-pressure turbine geometry operating in subsonic flow. Combustor hot streaks were included in the simulations. The radial location and the clocking position of the hot streak were varied across the inlet relative to the first-stage stator.

Nomenclature

a	= speed of sound
F, G, H	= x, y, and z components of flux
P	= static pressure
Q	= vector of flow variables
q	= heat flux per unit area, $q = -k(\partial T/\partial n)$
T	= static temperature
U	= rotor velocity
u, v, w	= x, y, and z components of velocity
μ	= viscosity
ρ	= density
Ω	= rotor rotational speed

Subscripts

hs	= hot streak
i	= inviscid quantity
m	= midspan value
n	= normal direction
T	= turbulent quantity
t	= stagnation quantity, time derivative
v	= viscous quantity
x, y, z	= first derivative with respect to x, y, and z
1	= first stator inlet quantity
2	= rotor inlet quantity
3	= rotor exit quantity
4	= second stator exit quantity
∞	= freestream quantity

Introduction

HOT streaks are known to have a significant impact on the wall temperature distributions of first-stage turbine rotors. The experimental geometry most often employed to simulate hot streak migration is the large-scale rotating rig (LSRR) turbine model used by Butler et al.[1] and Roback and Dring.[2] The LSRR is a large-scale, low-speed, rotating-rig wind-tunnel facility designed to simulate the flowfield in an axial-flow turbine. The migration of hot streaks through the LSRR has been simulated by many researchers, including Krouthen and Giles,[3] Rai and Dring,[4] Takahashi and Ni,[5,6] Dorney et al.,[7] Dorney and Davis,[8] Dorney and Gundy-Burlet,[9] and Gundy-Burlet and Dorney.[10] Although these numerical simulations have produced significant insights into the mechanisms controlling hot streak migration, there is still a significant amount of research needed to formulate design criteria for controlling the adverse effects of hot streaks.

The focus of the present effort has been to study the effects of varying the radial and circumferential locations of hot streaks at the inlet to a high-pressure turbine, with the goal of developing passive and inexpensive techniques for controlling the adverse effects caused by the hot streaks. A three-dimensional, unsteady Navier–Stokes analysis has been used to study the $1\frac{1}{2}$-stage configuration of the LSRR turbine. The hot streak was located at three separate radial locations and two different circumferential (clocking) positions at the inlet to the first-stage stator. The time-averaged and unsteady temperature data have been used to analyze the effects of hot streak placement on the heating of turbine airfoils.

Algorithm

The current work is based on an extension of an approach developed by Rai and is discussed in detail in the work of Rai[11] and Rai et al.[12] The approach is reviewed in brief here. The flowfield is divided into two basic types of zones. Inner O grids are used to resolve the flowfield near the airfoils. These O grids are overlaid on outer H grids that are used to resolve the flowfield in the passages between airfoils. The H grids are allowed to slip relative to one another to simulate the relative motion between rotors and stators. The thin-layer Navier–Stokes equations[13] are solved in all zones. The governing equations are cast in the strong conservation form. A fully implicit, finite difference method is used to advance the solution of the governing equations in time. Adiabatic boundary conditions are enforced at all wall boundaries. A Newton–Raphson subiteration scheme is used to reduce the linearization and factorization errors at each time step. The convective terms are evaluated using a third-order-accurate, upwind-biased Roe[14] scheme. The viscous terms are evaluated using second-order-accuratecentral differences. The Baldwin–Lomax[13] turbulence model is used to compute the turbulent eddy viscosity. Details of the turbulence model, zonal and natural boundary conditions, grid configuration, bookkeeping system,

Received 12 September 1998; revision received 20 May 1999; accepted for publication 20 June 1999. This material is declared a work of the U.S. Government and is not subject to copyright protection in the United States.

*Deputy Branch Chief, Computational Physics and Simulations Branch. Senior Member AIAA.

†Associate Professor, Department of Mechanical Engineering. Senior Member AIAA.

and database management systems are discussed by Gundy-Burlet and Dorney[10] and Gundy-Burlet et al.[15]

Geometry and Grid

The three-dimensional turbine model is based on the LSRR geometry used in the experiments performed by Dring et al.[16,17] and Joslyn and Dring.[18] The LSRR is a $1\frac{1}{2}$-stage turbine with a 27-in. midspan radius, 6-in. span, and airfoil aspect ratios of approximately unity. The turbine hub and casing are at constant radii. The axial gap between the first stator and rotor is approximately 50% of the first-stage average axial chord, whereas the gap between the rotor and the second stator is approximately 67% of their average chord. The rotor tip clearance is approximately 1% of span. A large experimental database exists for this turbine, including time-averaged pressures at several spanwise locations on each airfoil, traverse data behind each airfoil, and surface flow visualizations.

The experimental configuration has 22 airfoils in the first stator row and 28 airfoils in each of the rotor and second-stage stator rows, for a total of 78 airfoils. A three-dimensional computation of the flow through the complete turbine configuration would be prohibitively expensive. To reduce the cost of the computation, the number of stators in the first row was increased to 28, and the size of the stators was reduced by a factor of 22/28 to maintain the same blockage. The flow is then assumed to be periodic from passage to passage, thereby allowing a reduction to a single blade or vane in each of the rows.

The grids used to describe the hub and airfoil surfaces of the turbine are shown in Fig. 1. The stator O grid contains 214 points in the wrap-around direction, 26 points in the surface-normal direction, and 51 points in the radial direction. The rotor O grid contains 214 points in the wrap-around direction, 45 points in the surface-normal direction, and 51 points in the radial direction. The additional points in the rotor grid exist to discretize the rotor tip region. The dimensions of the H grids vary, but average 123 points in the axial direction, 81 points in the circumferential direction, and 51 points radially. The dimensions of the H grids used to discretize the inlet and outlet regions of the turbine stage are $34 \times 81 \times 51$. These relatively fine grid dimensions were arrived at through the use of a two-dimensional code used to evaluate the grid density needed to support the convection of the wakes with minimal dissipation. The total number of grid points used for the grid system was approximately 2.7×10^6.

Numerical Results

The inlet Mach number to the first-stage stator was 0.07, and the inlet flow was assumed to be axial. The rotor rotational speed was 410 rpm. The freestream Reynolds number was 39,370/cm. The midspan pressure coefficient at 14% of the chord aft of the second-stage stator trailing edge was $C_{p_{\text{exit}}} = -9.395$, where C_p is defined as $C_p = (P - P_{t1})/(0.5 \times \rho_1 \times U_m^2)$. The hot streak temperature was chosen to be 1.2 times the temperature of the freestream inlet flow. Actual hot streak temperatures 1.1–1.6 of the temperature of the freestream are typical of engine operating environments (R. K. Takahashi, Pratt and Whitney, August 1996, private communication).

Comparisons of the predicted time-averaged and unsteady pressure distributions with experimental data were presented in Refs. 10 and 19, and are not repeated here. The method for estimating the grid density requirements was based on the work in Ref. 20, in which a detailed grid resolution study was performed to determine the grid resolution needed to predict accurately both aerodynamic and heat transfer quantities.

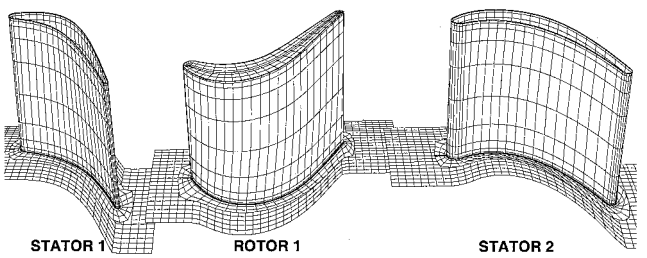

Fig. 1 Zonal grid topology.

To study the effects of radial placement, a hot streak was introduced at 20, 40, and 60% of the span at the inlet to the first stator. In addition, simulations were performed in which the hot streak was 1) directly aligned (fully impinging) with the first-stage stator, and 2) introduced midpassage (nonimpinging) between adjacent first-stage stator airfoils (see Dorney and Gundy-Burlet[9] for the importance of the relative position between the hot streak and first-stage stator and the effects on rotor heating). Thus, a total of six computations were performed.

These numerical simulations were run at 2000 time steps (with two Newton subiterations at each time step) per cycle on the Cray J90 supercomputer at NASA Ames Research Center. A cycle corresponds to the rotor blade rotating through an angle of $2\pi n/N$, where n is the number of stator blades (i.e., $n = 1$) used in the simulation and N is the number of stator airfoils in the modeled machine, that is, $N = 28$. The code was benchmarked at 31 μs/iteration/grid point and 384 megafloating point operations per second (MFLOPS) on a Cray C90.

Figures 2–8 show surface temperatures. Figs. 2, 3, and 5–8 show instantaneous surface temperatures and an instantaneous isocontour of temperature ($T/T_\infty = 1.08$, colored red) for each of the six hot streak inlet positions. In these Figs. 2, 3, and 5–8, the change in color on the surface from blue to red indicates an increase in surface temperature. The same color map was used for each of Figs. 2, 3, and 5–8 so that surface temperatures can be easily compared between all of the images. Each figure consists of two views of the turbine, and all of the views have the inlet flow entering from the left. The upper image displays the suction surface of the rotor and the pressure surfaces of the stators. In the lower image, the suction surfaces of the stators and the pressure surface of the rotor are seen. The 20% midpassage case is shown in Fig. 2. The hot streak flows smoothly between adjacent first-stage stators (stator 1) and enters the rotor passage still essentially intact near the 20%-span station. On the suction side of the rotor, a fragment of the hot streak can be seen convecting along the surface and extending down into the hub endwall region, causing hub surface temperatures on par with those of the rotor airfoil suction surface. The lower image shows the classic migration of the hot streak toward the pressure surface of the rotor and the typical spreadout and buildup of hot streaks from successive cycles. The hot streak moves toward the hub and spreads down into the hub boundary-layer region. The hot streak induces higher hub temperatures that extend through the second-stage stator (stator 2) passage.

In Fig. 3, instantaneous surface temperatures and isotherms can be seen for the directly impacting 20%-span case. On the pressure surface of stator 1, the hot streak spreads out radially toward the hub and continues to spread through the hub boundary layer toward the suction surface of the adjacent stator. The entrainment of the hot streak in the hub boundary layer continues until it is convected into the rotor passage, where the rotor passing and the leading-edge horseshoe vortex sufficiently energize the boundary layer to mix out this leg of the hot streak. The part of the hot streak convecting along the stator 1 suction surface becomes entrained in the trailing-edge shedding and is partially mixed out by the time it reaches the rotor surface. The hot streak is redirected toward the rotor suction surface, so that pressure surface temperatures are significantly lower than they are for the case shown in Fig. 2. Because the hot streak is partially mixed out by the time it reaches the rotor, surface temperatures in the rotor and stator 2 passages, particularly in the hub region, are significantly lower for the 20% directly impacting case than for the 20% midpassage case. This is at the expense of much higher heating in the hub endwall region in the stator 1 passage.

These observations are supported through inspection of the time-averaged temperatures on the hub surface for the 20%-span cases in Fig. 4. Discontinuities occur at the slip boundaries because the temperature is time averaged relative to the local airfoil frame of reference. When the hot streak is introduced at midpassage and 20%

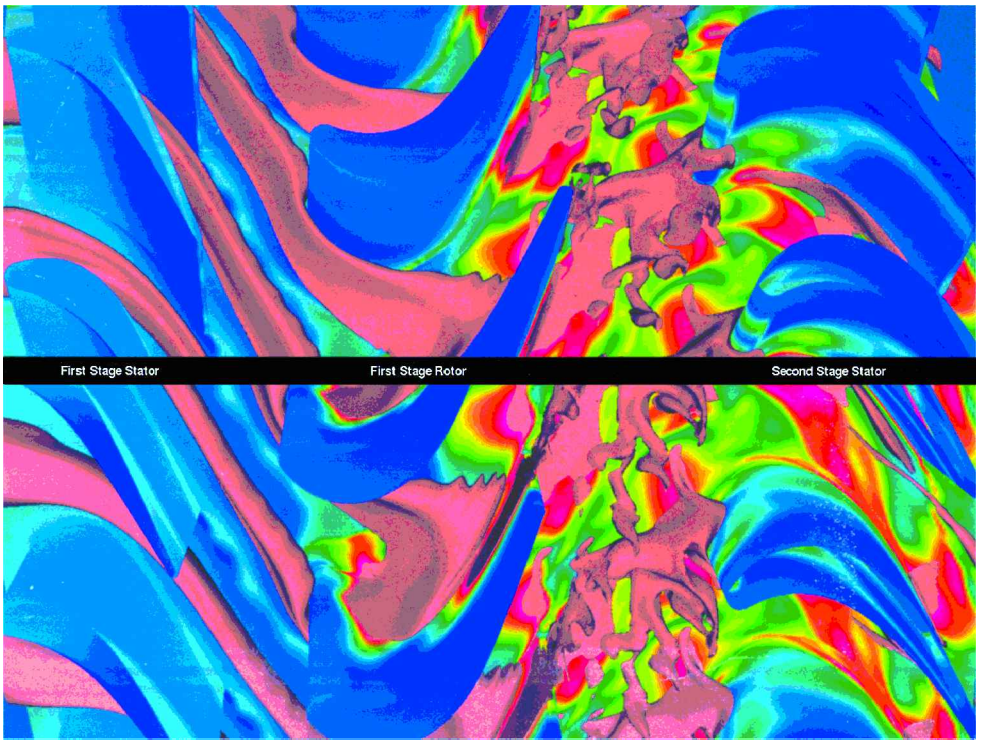

Fig. 2 Instantaneous surface temperature and isotherm: hot streak at midpassage and 20% span.

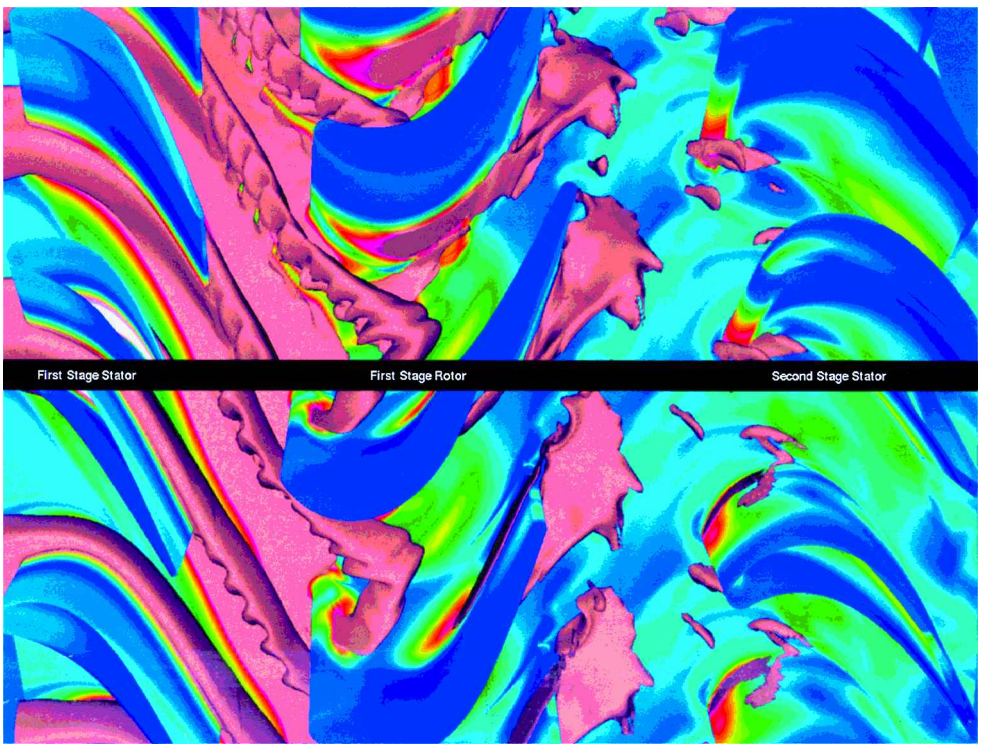

Fig. 3 Instantaneous surface temperature and isotherm: hot streak directly impacting and 20% span.

span (upper image), hub temperatures within the stator 1 passage are near freestream, but become significant near the trailing-edge rotor pressure surface region. Hot streak clocking effects become evident in the stator 2 passage. The hot streak appears to directly impact stator 2 and is entrained in the horseshoe vortex leading to significant time-averaged surface temperatures in the stator 2 leading-edge region. The lower image shows the time-averaged hub surface temperatures for the directly impacting 20%-span case. The hot streak is concentrated on the pressure surface side of stator 1 and can be seen to be migrating toward the suction side through the boundary layer. The high, time-averaged temperatures extend into the rotor passage where they substantially mix out through their interaction with the rotor horseshoe vortex. Peak time-averaged surface temperatures for this case are on the order of the freestream hot streak temperature. However, the hot streak remains in a stable location, which has implications for developing successful cooling strategies.

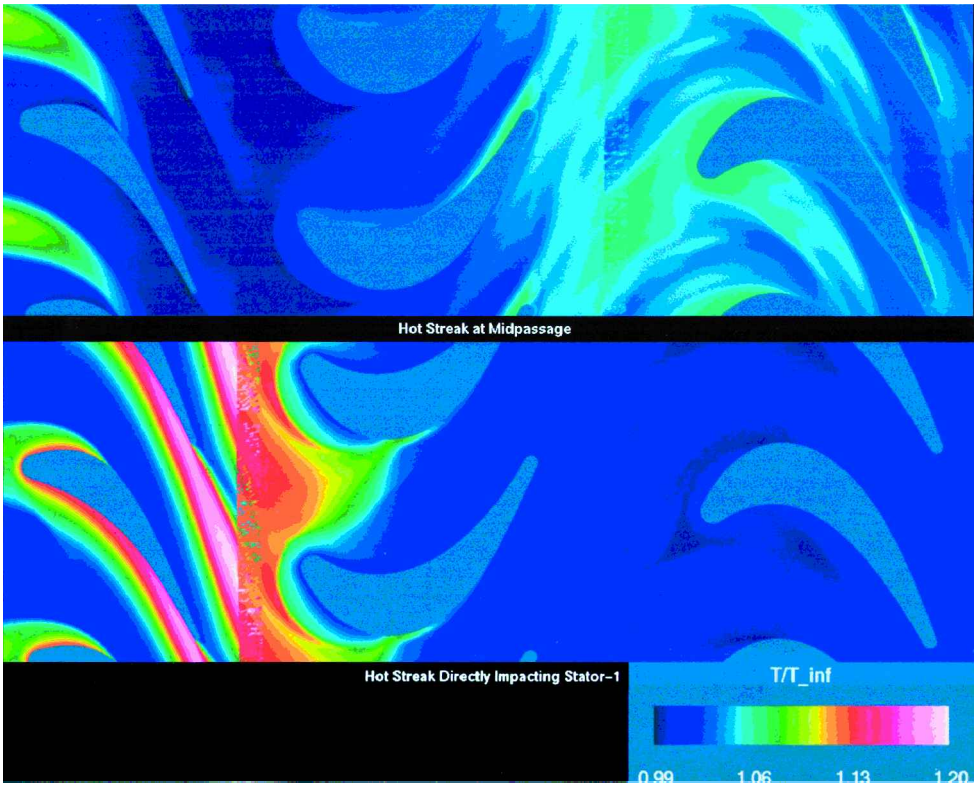

Fig. 4 Time-averaged surface temperature on the hub: hot streak at 20% span.

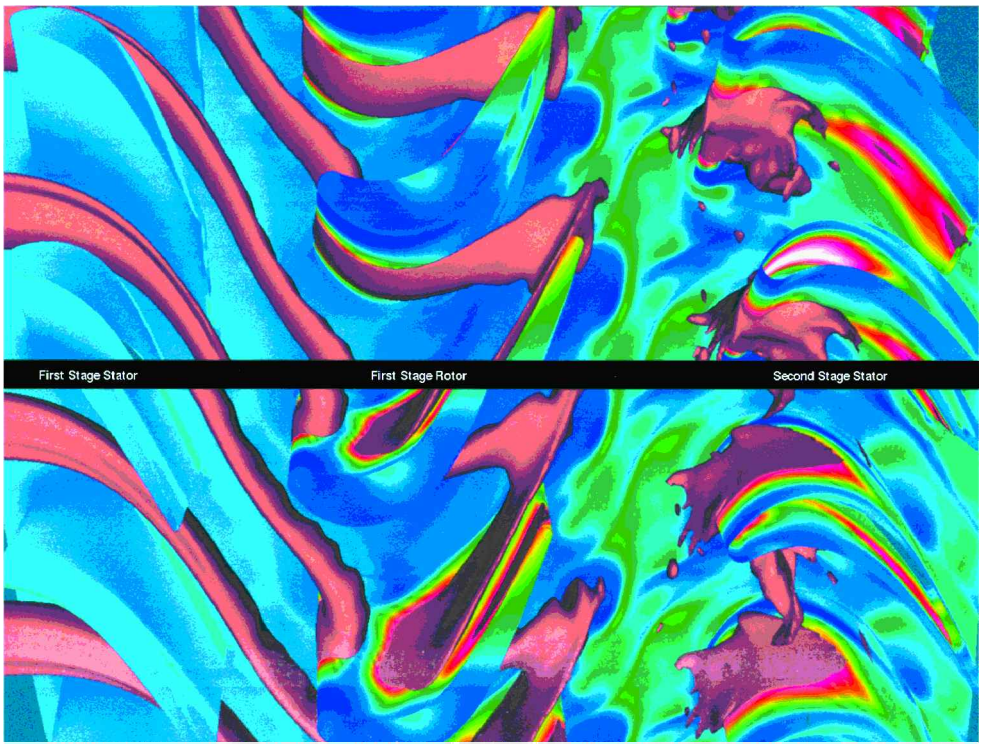

Fig. 5 Instantaneous surface temperature and isotherm: hot streak at midpassage and 40% span.

Instantaneous surface temperatures and an isotherm for the 40%-span, midpassage case are shown in Fig. 5. The hot streak convects between adjacent stators and is relatively unaffected as it migrates toward the pressure surface of the rotor. It spreads radially over the pressure surface, with higher heating on the rotor tip than is seen in either of the 20% cases. The hot streak is chopped but convects fairly intact into the stator 2 passage where it induces significant heating on both surfaces of stator 2. The effect of the hot streak is primarily felt in the midspan region throughout the machine.

Similar data for the 40%-span, directly impacting case are shown in Fig. 6. The hot streak impacts stator 1 at a well-defined, spanwise location and convects downstream to be entrained in the vortex shedding off the trailing edge of stator 1. This entrainment partially mixes out the hot streak by the time it impacts the rotor. The extent of the elevated surface temperatures on the rotor are reduced

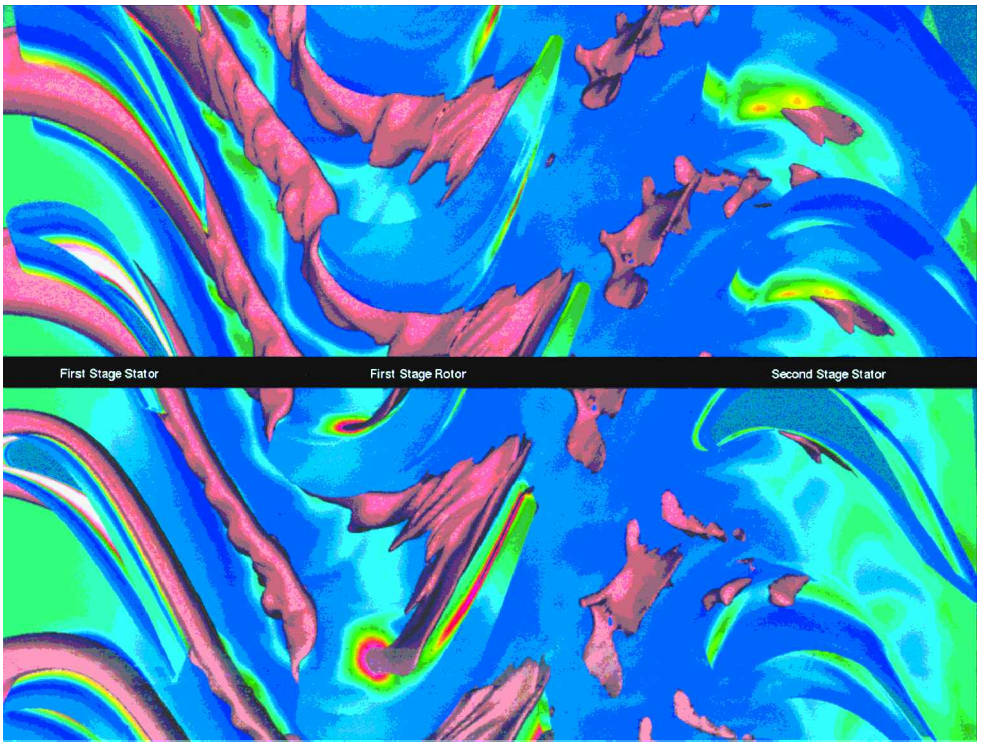

Fig. 6 Instantaneous surface temperature and isotherm: hot streak directly impacting and 40% span.

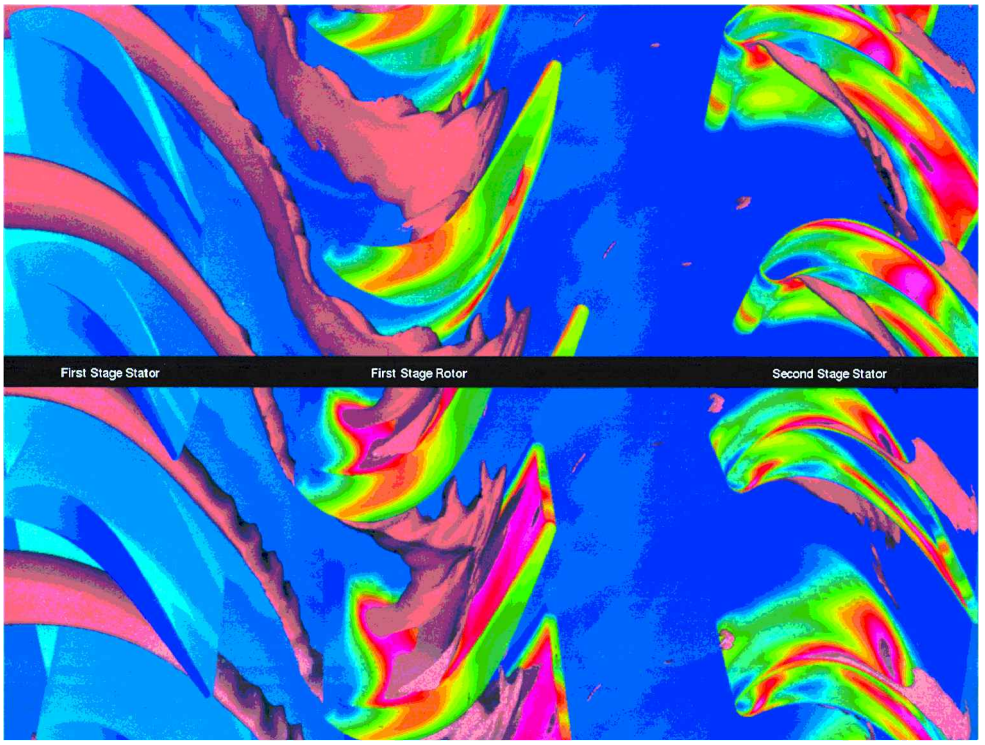

Fig. 7 Instantaneous surface temperature and isotherm: hot streak at midpassage and 60% span.

as compared to those for the 40%-midspan case, and surface temperatures on stator 2 are nearly freestream. The hot streak again is largely limited to the midspan region of the turbine.

Figure 7 shows instantaneous surface temperatures and an isotherm for the 60%-span midpassage case. In this case, even though the hot streak is not directly impacting the stator surface, the hot streak is affected more by the stronger secondary flows near the stator 1 outer casing than it is in the other midpassage cases. It appears to neck down more and can be seen to interact with the trailing-edge shedding from stator 1. It also appears to twist in the passage because it is affected by the outer casing secondary flows of stator 1. Even though the isotherm value chosen for these images does not appear in the rotor tip region, surface temperatures on the tip are higher than for any case presented thus far. The hot streak is entrained in the tip leakage flow and convects to the suction surface of the rotor, where it increases surface temperature. Significant

surface temperatures are evident in the outer casing region of stator 2, and a hot streak remnant can be seen convecting along the outer casing in the stator 2 passage.

The 60% directly impacting case is presented in Fig. 8. Here, the isotherm can be seen spreading radially over stator 1 to within approximately 5% of the span of the casing. The entrainment of the hot streak within the trailing-edge shedding of stator 1 can clearly be seen, and the hot streak twists with the outer casing secondary flow as it convects toward the rotor. Surface temperatures on the rotor indicate a fair amount of mixing-out in the parts of the hot streak convecting through the core flow. However, part of the isotherm convects sufficiently close to the tip casing that it is eventually entrained in the rotor tip leakage flow. Remnants of the isotherm extruded through the rotor tip region can be seen convecting along the casing outside of the boundary layer. The surface temperature for stator 2 is elevated slightly in the extreme tip region.

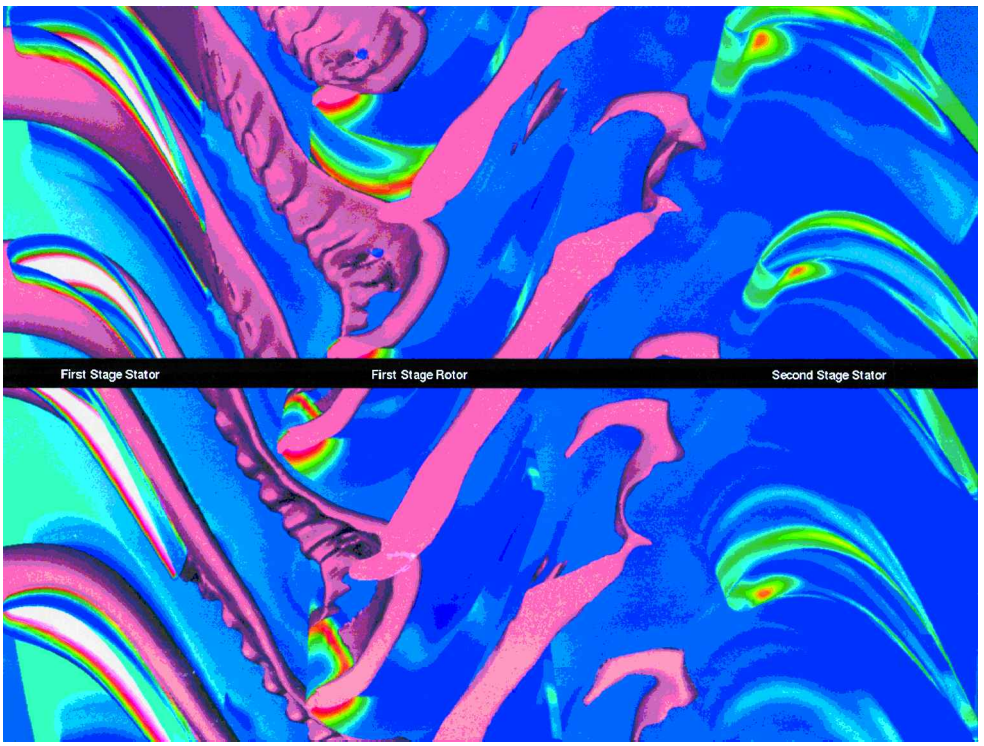

Fig. 8 Instantaneous surface temperature and isotherm: hot streak directly impacting and 60% span.

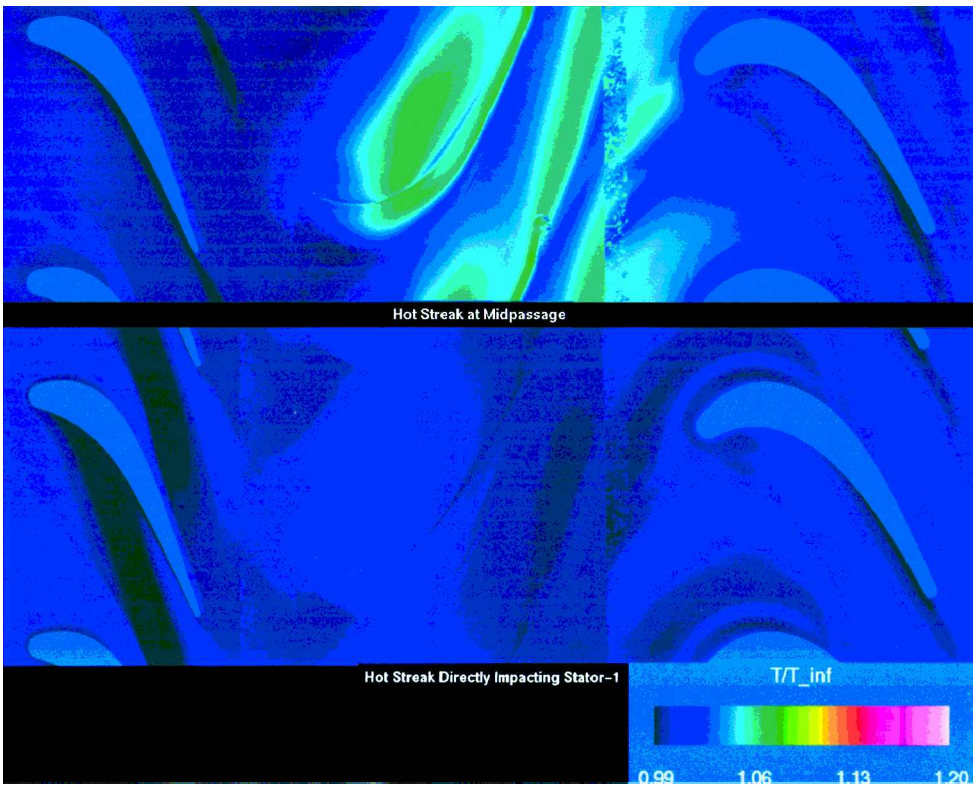

Fig. 9 Time-averaged surface temperature on the outer casing: hot streak at 60% span.

Time-averaged surface temperatures for the casing are shown for the 60% midpassage (upper image) and 60% directly impacting (lower image) cases in Fig. 9. The casing surface temperature is significantly increased in the rotor passage for the midpassage case. The elevated temperatures persist into the stator 2 passage, where clocking effects become evident. The hot streak remnant is striking the suction side of the leading edge of stator 2. The case with the hot streak directly impacting stator 1 at 60% span indicates that the hot streak has been sufficiently mixed-out and redirected so that no significant heating occurs on the casing.

Figures 10–15 show contours of the time-averaged surface temperatures overlaid with time-averaged particle traces on the suction and pressure surfaces of each airfoil for all six hot streak positions. Note that the colors associated with each contour value are the same for Figs. 10–15. Black is associated with the lowest temperatures, and white indicates the highest temperatures. The flow

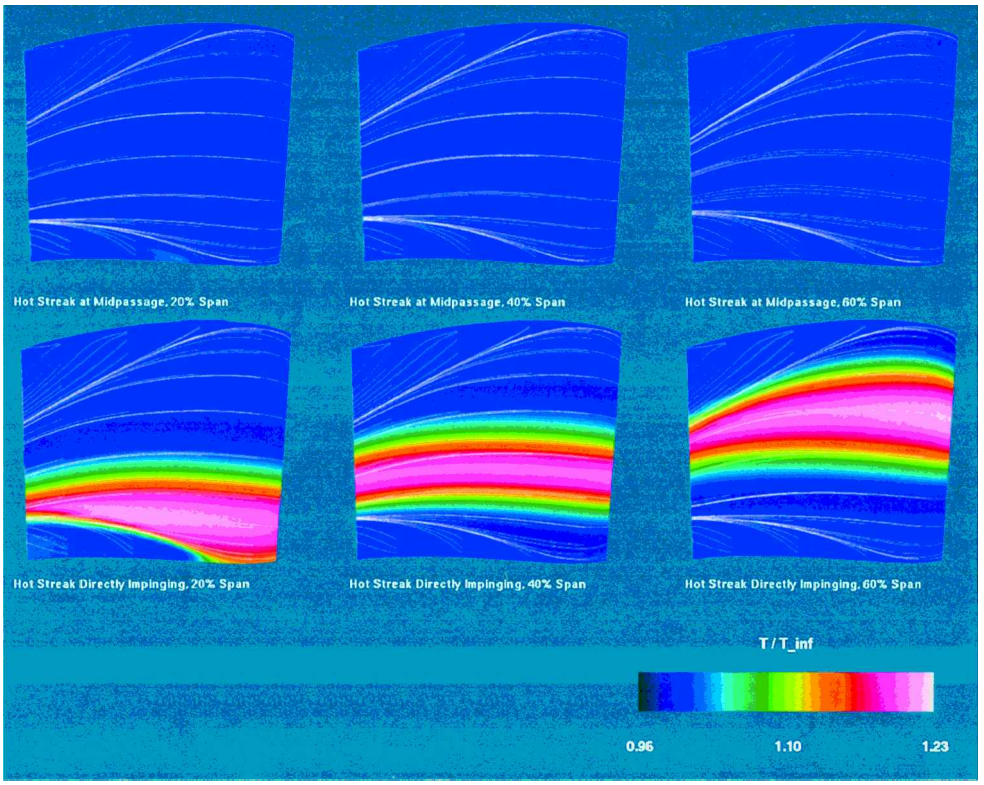

Fig. 10 Time-averaged surface temperature: suction surface of first-stage stator.

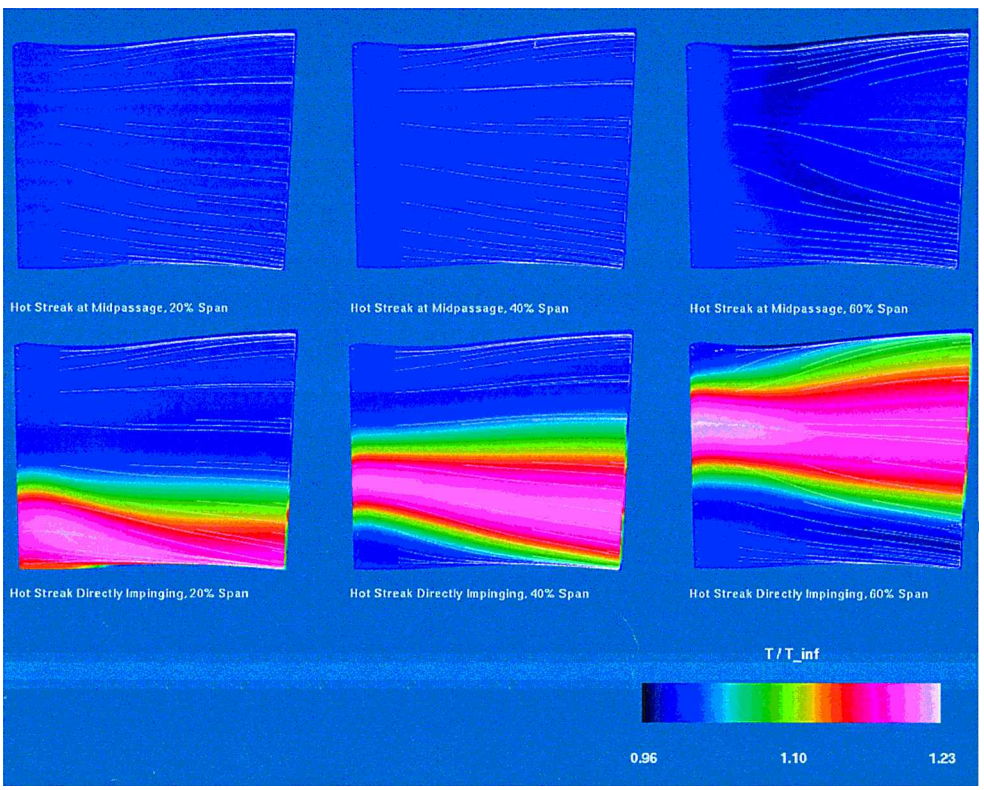

Fig. 11 Time-averaged surface temperature: pressure surface of first-stage stator.

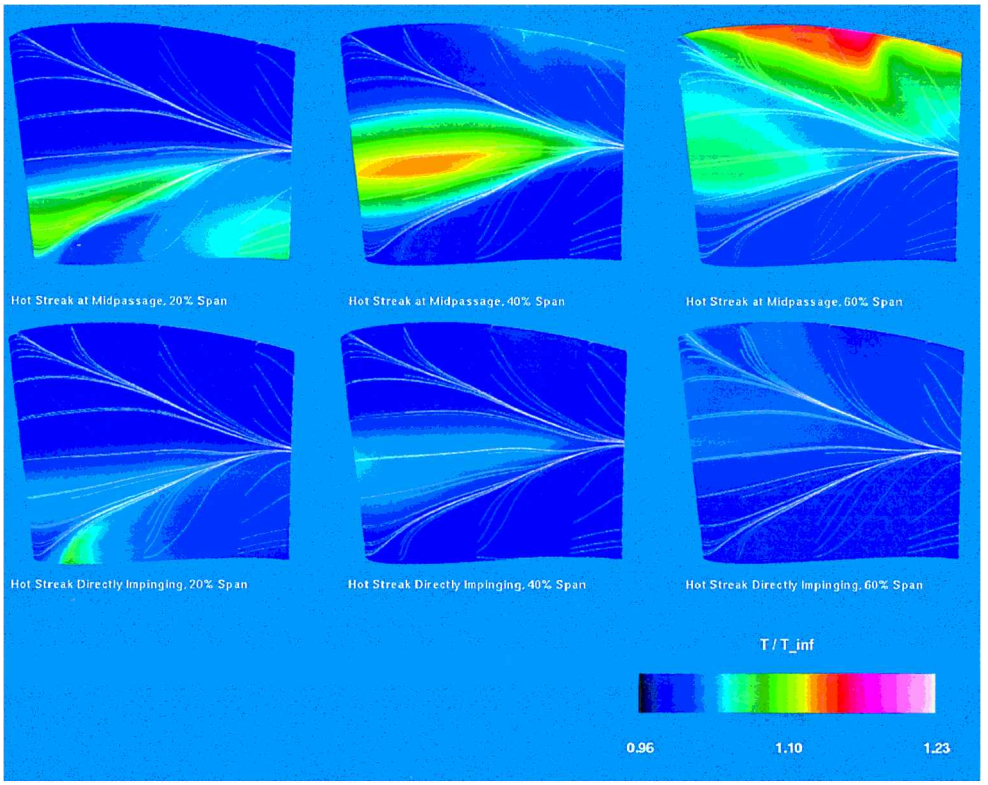

Fig. 12 Time-averaged surface temperature: suction surface of first-stage rotor.

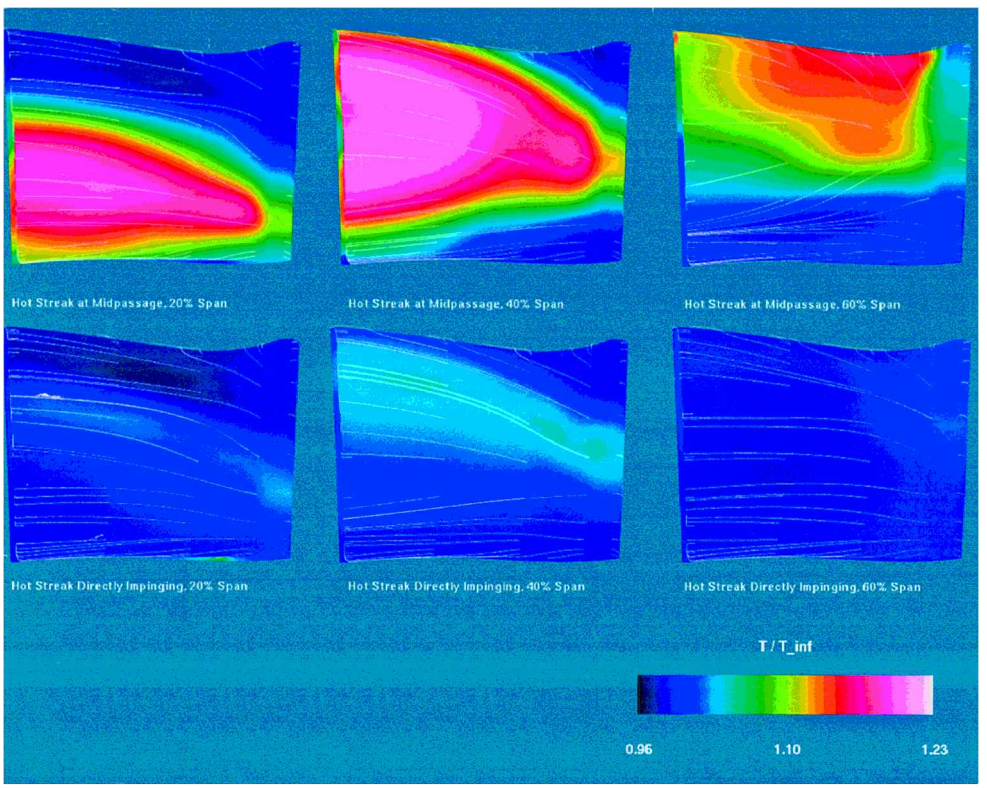

Fig. 13 Time-averaged surface temperature: pressure surface of first-stage rotor.

is from right to left in Figs. 10, 13, and 14 (so that the blade and vane leading edges are on the right) and goes from left to right in Figs. 11, 12, and 15 (so that the leading edges are on the left).

Figure 10 shows contours of the time-averaged temperature overlaid with the time-averaged particle traces on the suction surface of the first-stage stator for each of the six simulations. For the cases in which the hot streak directly impacts the first-stage stator, there is a substantial surface temperature increase due to the hot streak, and it clearly reflects the radial span station at which the hot streak was introduced. When the hot streak is introduced at 20% span and impinges on the stator, the hub secondary flows prevent the heated fluid from penetrating into the trailing-edge surface hub end wall region. A similar effect is seen for the 60% fully impinging case where the shroud secondary flow limits the radial extent of the surface imprint of the hot streak. It is observed that, when the hot streak is introduced

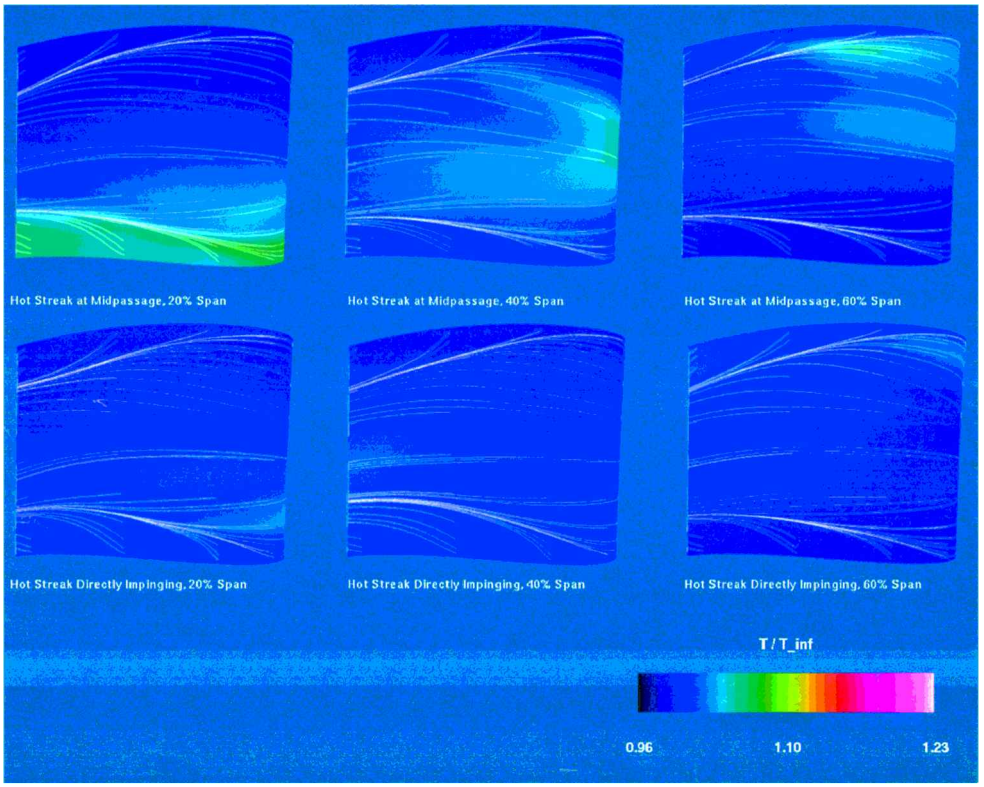

Fig. 14 Time-averaged surface temperature: suction surface of second-stage stator.

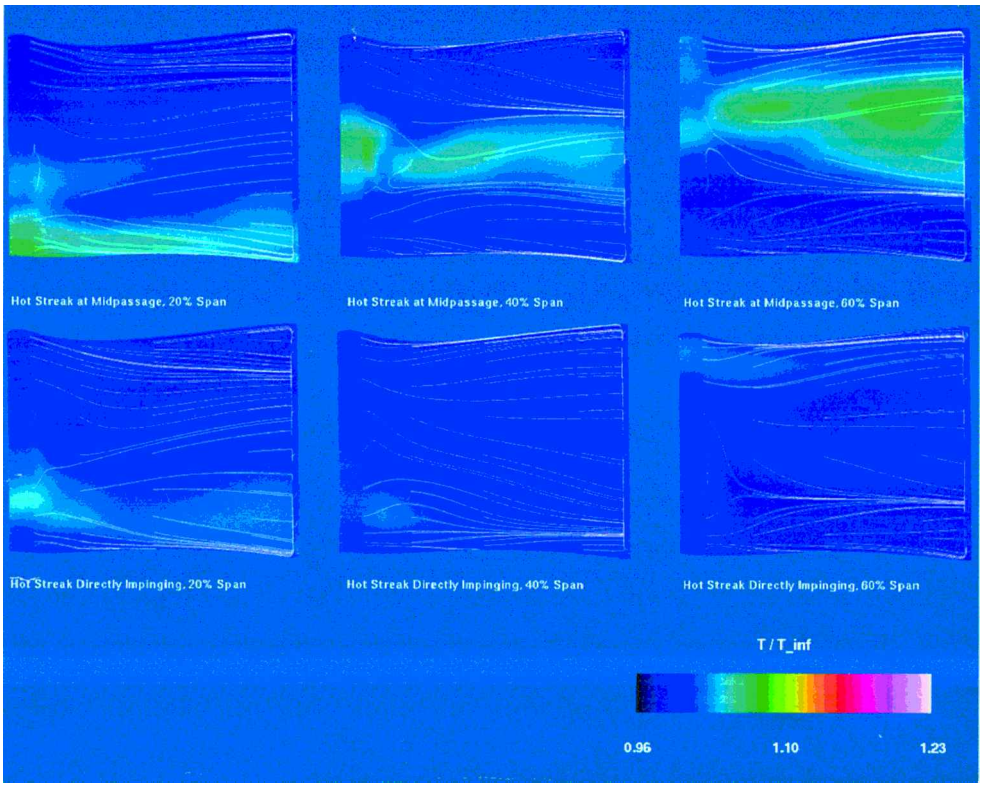

Fig. 15 Time-averaged surface temperature: pressure surface of second-stage stator.

at 60% span and midpassage, the shroud endwall secondary flows become stronger.

Figure 11 shows contours of the time-averaged surface temperature on the pressure surface of the first-stage stator. When the hot streak is introduced directly impacting stator 1 at 20% span, the hot streak interacts with the endwall flow to redirect the flow and itself toward the hub. In Fig. 3, the hot streak was seen migrating onto the hub, verifying this assessment. The particle traces are also slightly redirected in the 40% directly impacting case relative to the 40% midpassage case. In the 60% fully impinging case, the hot fluids migrate radially toward both the shroud and hub endwalls. It is also evident, especially when the hot streak is introduced at 60% span, that the velocity jet associated with the hot streak has a significant impact on the direction of the streamlines. In general, it appears that introducing the hot streak at 60% span, and impinging it on the stator, causes

the greater heating over more of the surface than do the other cases.

The time-averaged surface temperatures on the suction surface of the rotor are shown in Fig. 12. All of the cases indicate the presence of strong endwall secondary flows. It is observed in the 40% midpassage case that the endwall flows pinch off the hot streak at approximately 80% of the axial chord. This phenomenon was observed in both the experiments of Butler et al.[1] and the simulations of Dorney et al.[7] The 40% midpassage case also exhibits heating in the trailing-edge tip region that is caused by hot fluid leaking over from the pressure surface of the airfoil. The results of the 20% midpassage simulation show elevated surface temperatures in the lower half-span, with some of the hot streak becoming entrained in the hub secondary flows. The most severe surface heating occurs when the hot streak is introduced at 60% span and midpassage. In this case, the entire outboard and tip region of the pressure surface exhibit very high time-averaged temperatures. Part of the heating is caused by leakage of hot fluid from the suction surface to the pressure surface, whereas some of the heating is a result of the hot streak mixing with the tip clearance vortex. In operation, this type of surface heating would probably lead to premature blade failure in the tip region. All of the cases where the hot streak fully impinges on the first-stage stator show much less surface heating than do the midpassage cases. The impinging cases also show much less leakage of hot fluid from the suction surface of the rotor.

Figure 13 shows contours of the time-averaged surface temperatures on the pressure surface of the rotor. The rotor pressure surface is traditionally the region subjected to the highest time-averaged surface temperatures. As expected, the cases where the hot streak is introduced midpassage between two first-stage stators exhibit the most severe surface heating. The 40% midpassage simulation shows the hot streak fluid migrating radially towards both the hub and tip endwalls. The radial migration of the hot fluid along with the low convection velocities on the pressure side of the rotor passage combine to generate high, time-averaged temperatures. The 20% midpassage solution indicates a significant region of elevated temperatures, although these temperatures are lower than those in the 40% midpassage case. The 60% midpassage solution shows less surface heating than there is in the 20 and 40% midpassage cases, but from a durability aspect the heating at the tip would probably still be a concern. Note that the hot streak significantly alters the direction of the fluid streamlines. Similar to the results presented in Refs. 9 and 10, the results of the fully impinging cases show much less airfoil surface heating than do the midpassage cases. In particular, the cases where the hot streak is introduced at 20 and 60% span show minimal surface heating of the airfoil surface as the hot streak is partially mixed-out and redirected toward the hub and tip casings, respectively.

The time-averaged surface temperatures on the suction surface of the second-stage stator are shown in Fig. 14. The midpassage cases again show higher surface temperatures than do the impinging cases. The 20% midpassage case in particular shows significantly elevated temperatures in the hub endwall region. Note that even after passing through the two blade rows and migrating radially on pressure surface of both the first-stage stator and rotor airfoils, the high-temperature regions in the midpassage cases are still close (radially) to their original introduction locations. Only nominal heating is observed on the suction surface in the impinging solutions.

The time-averaged surface temperatures on the pressure surface of the second-stage stator are shown in Fig. 15. The midpassage cases shown suggest that the hot streak fluid undergoes a redistribution process in the second-stage stator passage, similar to that in the rotor passage. This finding agrees with the results of Ref. 21, but stand in contrast to those of Ref. 6. The same blade count ratios were used in this study and Ref. 21, whereas a different ratio was used in Ref. 6, suggesting that temperature redistribution in downstream stages may be a function of the airfoil counts. Similar to the pressure surface, the impinging cases show little surface heating.

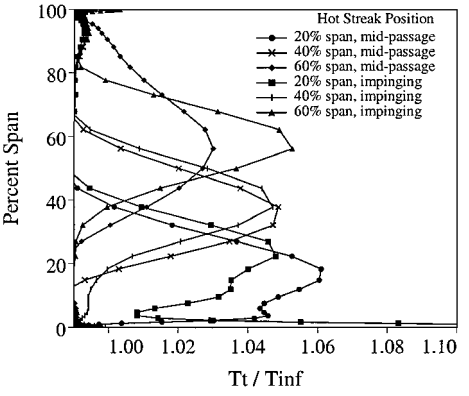

Fig. 16 Radial profiles of T_t aft of stator 1.

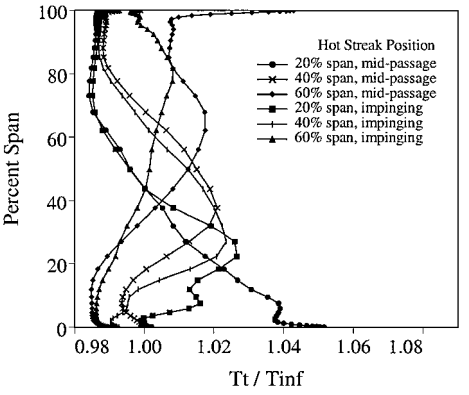

Fig. 17 Radial profiles of T_t aft of rotor 1.

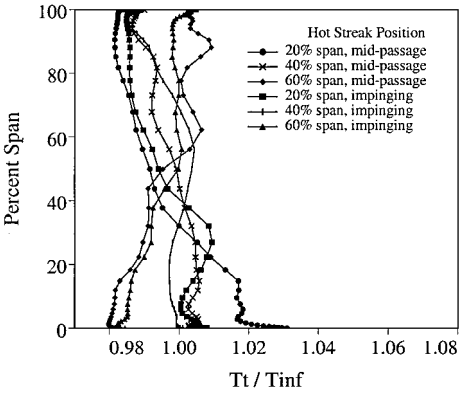

Fig. 18 Radial profiles of T_t aft of stator 2.

Figures 16–18 contain time- and circumferentially averaged radial profiles of the total temperature at the exit of each blade row. At the exit of the first-stage stator (Fig. 16), the peak total temperatures are greater in the nonimpinging calculations with the exception of the 60%-span case. Inspection of Figs. 7 and 8 indicates that the secondary flows concentrate the core of the isotherm for the impacting case and neck it out for the midpassage case. A redistribution of the hot streak onto the tip case can be seen for the 60% impacting case. The effect of the entrainment of the hot streak in the hub secondary flow can be seen in the 20%-span impinging case. The imprint of the hot streak as it migrates from the pressure side of stator 1 to the hub boundary layer can clearly be seen in the elevated total temperature values at the hub. The peak temperature of $T/T_\infty = 1.11$ near the hub for this case is substantially elevated over all other cases for this axial location.

At the exit of the rotor (Fig. 17), the high total temperatures exhibited near the hub for the 20% directly impacting case have been substantially mixed-out through the interaction with the flows induced by the rotor and rotating hub. The peak total temperatures now occur for the 20%-span midpassage case, and this case now shows a migration of the hot streak toward the hub. The results of the cases in which the hot streak is introduced at midspan indicate that the hot streak has only minimally interacted with the secondary flows at either end wall. The 60% midpassage case exhibits a redistribution of the hot streak into the tip casing boundary-layer flow. The total temperatures at the exit of stator 2 (Fig. 18) indicate that the peak total temperature still occurs for the 20% midpassage case and that the peak total temperatures are concentrated at the hub.

Conclusions

Previous numerical and experimental studies have shown that combustor hot streaks can cause significant temperature increases along the pressure surface of first-stage turbine rotors. In the current investigation, the effects of combustor hot streaks have been studied for a group of six parametric cases, that is, fully impinging and midpassage hot streaks introduced at 20, 40, and 60% of span. Based on the matrix of simulations the following conclusions have been drawn:

1) Direct impingement of the hot streak on the first-stage stator increases the heat load on this airfoil, but significantly reduces the heat load on the rotor and second-stage stator. This condition should be acceptable because first-stage stators are normally designed to withstand these high temperatures (through the use of film cooling, etc.).

2) The increased heat load (associated with impinging the hot streak) on the first-stage stator does not vary significantly with time. This should allow the use of film cooling schemes that minimize the amount of wasted cooling flow.

3) Impingement of the hot streak on the first stator in the hub region causes migration of the hot streak from the stator pressure surface into the hub boundary layer and induces substantial, but stable in time, heating of the hub in the stator 1 passage.

4) Introducing the hot streak at midspan and midpassage results in less end wall heating but generates severe heat loads on the pressure surface of the rotor.

5) Placement of the hot streak near the tip region causes increased time-averaged temperatures in a region already prone to burning and failure.

6) Impinging the hot streak on the first-stage stage stator desensitizes the rotor and second-stage stator heating patterns to the radial placement of the hot streak.

Based on these findings, we suggest introduction of the hot streak in the lower half-span of the airfoil passage, such that it impinges directly on the first-stage stator.

References

[1]Butler, T. L., Sharma, O. P., Joslyn, H. D., and Dring, R. P., "Redistribution of an Inlet Temperature Distortion in an Axial Flow Turbine Stage," *Journal of Propulsion and Power*, Vol. 5, No. 1, 1989, pp. 64–71.

[2]Roback, R. J., and Dring, R. P., "Hot Streaks and Phantom Cooling in a Turbine Rotor Passage: Part 1—Separate Effects," American Society of Mechanical Engineers Paper 92-GT-75, June 1992.

[3]Krouthen, B., and Giles, M. B., "Numerical Investigation of Hot Streaks in Turbines," AIAA Paper 88-3015, July 1988.

[4]Rai, M. M., and Dring, R. P., "Navier–Strokes Analysis of the Redistribution of Inlet Temperature Distortions in a Turbine," *Journal of Propulsion and Power*, Vol. 6, No. 3, 1990, pp. 276–282.

[5]Takahashi, R. K., and Ni, R. H., "Unsteady Euler Analysis of the Redistribution of an Inlet Temperature Distortion in a Turbine," AIAA Paper 90-2262, July 1990.

[6]Takahashi, R. K., and Ni, R. H., "Unsteady Hot Streak Migration Through a $1\frac{1}{2}$ Stage Turbine," AIAA Paper 91-3382, June 1991.

[7]Dorney, D. J., Davis, R. L., Edwards, D. E., and Madavan, N. K., "Unsteady Analysis of Hot Streak Migration in a Turbine Stage," *Journal of Propulsion and Power*, Vol. 8, No. 2, 1992, pp. 520–529.

[8]Dorney, D. J., and Davis, R. L., "Numerical Simulation of Turbine Hot Spot Alleviation Using Film Cooling," *Journal of Propulsion and Power*, Vol. 9, No. 3, 1993, pp. 329–336.

[9]Dorney, D. J., and Gundy-Burlet, K. L., "Hot Streak Clocking Effects in a $1\frac{1}{2}$ Stage Turbine," *Journal of Propulsion and Power*, Vol. 12, No. 3, 1996, pp. 619, 620.

[10]Gundy-Burlet, K. L., and Dorney, D. J., "Three-Dimensional Simulations of Hot Streak Clocking in a $1\frac{1}{2}$ Stage Turbine," *International Journal of Turbo and Jet Engines,* Vol. 14, No. 3, 1997, pp. 133–144.

[11]Rai, M. M., "Navier–Stokes Simulations of Rotor/Stator Interactions Using Patched and Overlaid Grids," *Journal of Propulsion and Power*, Vol. 3, No. 5, 1987, pp. 387–396.

[12]Rai, M. M., Madavan, N. K., and Gavali, S., "Multipassage Navier–Stokes Simulations of Turbine Rotor-Stator Interaction," *Journal of Propulsion and Power*, Vol. 9, No. 3, 1993, pp. 389–396.

[13]Baldwin, B. S., and Lomax, H., "Thin Layer Approaximation and Algebraic Model for Separated Turbulent Flow," AIAA Paper 78-257, Jan. 1978.

[14]Roe, P. L., "Approximate Riemann Solvers, Parameter Vectors, and Difference Schemes," *Journal of Computational Physics*, Vol. 43, No. 2, 1981, pp. 357–372.

[15]Gundy-Burlet, K. L., Rai, M. M., and Dring, R. P., "Two-Dimensional Computations of Multistage Compressor Flows Using a Zonal Approach," AIAA Paper 89-2452, July 1989.

[16]Dring, R. P., Blair, M. F., Joslyn, H. D., Power, G. D., and Verdon, J. M., "The Effects of Inlet Turbulence and Rotor/Stator Interactions on the Aerodynamics and Heat Transfer of a Large-Scale Rotating Turbine Model, i—Final Report," NASA CR-4079, May 1986.

[17]Dring, R. P., Blair, M. F., Joslyn, H. D., Power, G. D., and Verdon, J. M., "The Effects of Inlet Turbulence and Rotor/Stator Interactions on the Aerodynamics and Heat Transfer of a Large-Scale Rotating Turbine Model, iv—Aerodynamic Data Tabulation," NASA CR-4079, May 1986.

[18]Joslyn, H. D., and Dring, R. P., "Three Dimensional Flow and Temperature Profile Attenuation in an Axial Flow Turbine," Air Force Office of Scientific Research, Rept. R89-957334-1, March 1989.

[19]Gundy-Burlet, K. L., and Dorney, D. J., "Influence of 3D Hot Streaks on Turbine Heat Transfer," *International Journal of Turbo and Jet Engines,* Vol. 14, No. 3, 1997, pp. 123–132.

[20]Dorney, D. J., Ng, B. C., Al-Habbas, A., and Gundy-Burlet, K. L., "Numerical Simulations of Hot Streak Migration in a $1\frac{1}{2}$ Stage Turbine," AIAA Paper 95-0181, Jan. 1995.

[21]Dorney, D. J., and Davis, R. L., "Navier–Strokes Analysis of Turbine Blade Heat Transfer and Performance," *Journal of Turbomachinery,* Vol. 114, No. 4, 1992, pp. 795–806.

Color reproductions courtesy of Virginia Commonwealth University.